W. SWIDER

NRL Memorandum Report 3014

# Theoretical and Numerical Simulation Studies of Midlatitude F Region Irregularities

A. J. SCANNAPIECO AND S. R. GOLDMAN

*Science Applications, Inc.*
*McLean, Virginia*

and

S. L. OSSAKOW, D. L. BOOK, AND B. E. MCDONALD

*Plasma Dynamics Branch*
*Plasma Physics Division*

March 1975


**NAVAL RESEARCH LABORATORY**
**Washington, D.C.**

SECURITY CLASSIFICATION OF THIS PAGE *(When Data Entered)*

## REPORT DOCUMENTATION PAGE

READ INSTRUCTIONS BEFORE COMPLETING FORM

1. REPORT NUMBER: NRL Memorandum Report 3014
2. GOVT ACCESSION NO.:
3. RECIPIENT'S CATALOG NUMBER:

4. TITLE *(and Subtitle)*: THEORETICAL AND NUMERICAL SIMULATION STUDIES OF MIDLATITUDE F REGION IRREGULARITIES

5. TYPE OF REPORT & PERIOD COVERED: Interim report on a continuing NRL problem.

6. PERFORMING ORG. REPORT NUMBER:

7. AUTHOR(s): A.J. Scannapieco, S.L. Ossakow, S.R. Goldman, D.L. Book, and B.E. McDonald

8. CONTRACT OR GRANT NUMBER(s):

9. PERFORMING ORGANIZATION NAME AND ADDRESS: Naval Research Laboratory, Washington, D.C. 20375

10. PROGRAM ELEMENT, PROJECT, TASK AREA & WORK UNIT NUMBERS: NRL Problem A03-16, Project RR033-02-42-5308

11. CONTROLLING OFFICE NAME AND ADDRESS: Department of the Navy, Office of Naval Research, Arlington, Virginia 22217

12. REPORT DATE: March 1975

13. NUMBER OF PAGES: 29

14. MONITORING AGENCY NAME & ADDRESS *(if different from Controlling Office)*:

15. SECURITY CLASS. *(of this report)*: Unclassified

15a. DECLASSIFICATION/DOWNGRADING SCHEDULE:

16. DISTRIBUTION STATEMENT *(of this Report)*

Approved for public release; distribution unlimited.

17. DISTRIBUTION STATEMENT *(of the abstract entered in Block 20, if different from Report)*

18. SUPPLEMENTARY NOTES

19. KEY WORDS *(Continue on reverse side if necessary and identify by block number)*

F Region
Ionosphere
Irregularities
Nonlinear development

20. ABSTRACT *(Continue on reverse side if necessary and identify by block number)*

Numerical simulation results for the nonlinear evolution of F region irregularities using Perkins' [1973] model equations for the nighttime F region are given. The equilibrium we take, which satisfies the model equations, is that the F region Pedersen conductivity consists of a constant term plus a long wavelength variation in the east-west direction. The north-south short wavelength perturbation initially introduced is unstable to the E x B instability, if in addition to the supporting east-west electric field a north-south electric field, satisfying certain conditions, exists. The nonlinear results from such a system show sheet-like structures preferentially oriented

(Continues)

DD FORM 1 JAN 73 1473 EDITION OF 1 NOV 65 IS OBSOLETE
S/N 0102-014-6601



SECURITY CLASSIFICATION OF THIS PAGE *(When Data Entered)*

20. Abstract (Continued)

in the east-west direction, with a power spectrum, for the squared amplitude of the Pedersen conductivity fluctuations, proportional to $k^{-2}$ in the 1-30 km regime where the simulations were carried out. The power spectrum results are in good agreement with recent in situ observations from OGO 6 and ground based scintillation observations. The shape of the irregularities is in agreement with the midlatitude winter observations deduced from scintillation data by Singleton [1970].

CONTENTS

# THEORETICAL AND NUMERICAL SIMULATION STUDIES OF MIDLATITUDE F REGION IRREGULARITIES

## I. INTRODUCTION

Temperate – latitude spread F has been observed for many years (see Herman, 1966 for a comprehensive review). Recently, a model which attempts to describe the phenomenon has been provided by Perkins [1973]. Perkins derived a set of magnetic field line integrated moment equations (thus allowing variations only transverse to the geomagnetic field; see Section II) for the dynamical evolution of the nighttime F region. He showed that the equilibrium in which the nighttime F region is supported by $\underline{E} \times \underline{B}$ drifts is unstable, if in addition to the supporting eastward electric field, a north-south electric field exists. The instability takes the form of rising and falling sheets of ionization and his linear analysis showed a growth rate $\gamma \approx 3 \times 10^{-4} \nu_{in}^{-1}$ (where $\nu_{in}$ is the ion-neutral collision frequency at the F region peak). This can provide growth times of the order of a few minutes to an hour depending on whether the F layer is high or low. Perkins showed that the results of this instability generation mechanism were able to predict, albeit based on a linear analysis, several of the features observed in spread F.

In Perkins' derivation of the linear growth rate an equilibrium was taken where both the field line integrated Pedersen conductivity and field line integrated ion number density were assumed to have no horizontal gradients. However, as noted by Perkins [1973], this spread F instability will cause Pedersen conductivity gradients transverse to the magnetic field to be formed. These gradients should then be subject to the usual $\underline{E} \times \underline{B}$ instability (Simon, 1963, 1970; Linson and Workman, 1970).

Note: Manuscript submitted February 14, 1975.

It is the purpose of the present paper to extend the work of Perkins to the nonlinear development of a spatially varying ionospheric equilibrium. In particular, numerical simulation of Perkins' [1973] moment equations, with an initial equilibrium which has a long wavelength variation of the integrated Pedersen conductivity in the east-west direction and a shorter wavelength perturbation of this conductivity in the north-south direction, evolves to a quasi-final nonlinear state with the squared amplitude of the Pedersen conductivity fluctuations varying as $k^{-2}$ (where k is the magnitude of the wavevector). Such a power law for the F region irregularities is in good agreement with observations (Dyson et al., 1974; Rufenach, 1972).

This paper is divided into four sections. In Section II we present and discuss a set of moment equations first derived by Perkins [1973] which describes the dynamical behavior of the nighttime F region. In addition, a plausible equilibrium state is described and a linear perturbation analysis is carried out under conditions in which F region irregularities can develop. A delineation of the differences between our equilibrium and perturbation analysis and that of Perkins [1973] is presented in this section. In Section III numerical simulations of the nonlinear evolution of the dynamical equations for a portion of the nighttime F region are presented and discussed. Section IV contains a summary and further discussion of the results.

## II. MOMENT EQUATIONS: EQUILIBRIUM AND LINEAR ANALYSIS

The derivation of the moment equations presented here was first carried out by Perkins [1973]. We will not, therefore, rederive this set of equations, but reiterate the necessary assumptions made in their derivation. They represent a set of moment equations, in the electrostatic limit, for the magnetic field line integrated ion number density and Pedersen conductivity of the F region. The field line integrated potential is derived self-consistently from the vanishing of the divergence of the perpendicular current.

The assumptions made in the derivation of the set of equations are as follows: (1) the magnetic field is uniform and makes a dip angle D with the horizontal direction (see Figure 1); (2) E region contributions to the ionospheric conductivity are ignored; (3) recombination and ionization are neglected; (4) the neutral atmosphere consists of a single species distributed vertically with a scale height $H_n$; (5) both the falling of ions and horizontal drifts due to gravity are included; (6) the plasma is high enough so that the ion cyclotron frequency is greater than the ion-neutral collision frequency, $\Omega \gg \nu_{in}$; (7) the ions and electrons are isothermal; and (8) electric field and neutral winds give rise to Pedersen currents which can support the ionosphere by $\underline{j} \times \underline{B}$ forces. The geometry for the problem is given in Figure 1.

The equations can now be written as:

$$\frac{\partial N}{\partial t} + \nabla_x N(-\nabla_y \phi \frac{c}{B}) + \nabla_y N(\frac{g \cos D}{\Omega} + \nabla_x \phi \frac{c}{B}) = 0 \qquad (1)$$

$$\frac{\partial \Sigma}{\partial t} + \nabla_x \Sigma(-\nabla_y \phi \frac{c}{B}) + \nabla_y \Sigma(\frac{g \cos D}{\Omega} + \nabla_x \phi \frac{c}{B}) = \frac{e c \sin^2 D g N}{\Omega B H_n} \qquad (2)$$

$$+ \Sigma \nabla_y \phi \frac{c \cos D}{B H_n}$$

$$\nabla_{\perp} \cdot (\sum \nabla_{\perp} \phi) + \nabla_x \sum \cos D \left(\frac{2T}{e H_n} + \frac{mg}{e}\right) + \frac{2T}{e} \nabla_{\perp}^2 \sum - \nabla_y N$$

$$\cdot \frac{g e \cos D}{\Omega} = 0 \qquad (3)$$

where equations (1) and (2) represent the transport equations for the integrated number density and Pedersen conductivity respectively. The symbols used in equations (1), (2), and (3) are defined as follows:

$N$ = field line integrated ion number density

$\sum$ = field line integrated ion Pedersen conductivity

$\phi$ = field line integrated potential

$g$ = gravitational acceleration

$B$ = ambient geomagnetic field

$\Omega$ = ion cyclotron frequency

$H_n$ = neutral scale height

$m$ = ion mass

$D$ = magnetic dip angle

$e$ = electron charge

$T$ = temperature in units of energy

$\perp$ = direction transverse to $\underline{B}$.

Equation (3) is the equation for the potential obtained from

$$\nabla_{\perp} \cdot \underset{\sim}{J}_{\perp} = 0 \qquad (4)$$

where $\underset{\sim}{J}_{\perp}$ is the field line integrated current. It should be emphasized that equations (1) - (3) are two-dimensional, i.e., represent variations transverse to the ambient geomagnetic field.

In the predawn and post-sunset hours, gradients in the east-west direction will be formed and it must be shown that these gradients persist throughout the night. To show that these gradients do exist we will show that the set of moment equations yield a self-consistent

equilibrium when gradients of N and $\Sigma$ exist in the east-west or y direction. This represents a physical situation which is favorable for the development of the $\underline{E} \times \underline{B}$ gradient drift instability provided the east-west gradients persist and the ion-neutral relative drift is greater than a particular threshold value.

To do this assume that $\frac{\partial N_o}{\partial x} = \frac{\partial \Sigma_o}{\partial x} = 0$ and $\frac{\partial \phi_o}{\partial x} = -E_{ox}$, where subscript zero denotes equilibrium quantities. Thus, there are no north-south gradients in N and $\Sigma$, and a constant north-south electric field exists. Under these conditions the set of moment equations yield

$$\frac{\partial \Sigma_o}{\partial t} + \frac{\partial \Sigma_o}{\partial y}\left(\frac{g \cos D}{\Omega} - \frac{c E_{ox}}{B}\right) = \frac{e c g \sin^2 D}{\Omega B H_n} N_o + \Sigma_o \frac{\partial \phi_o}{\partial y} \frac{c \cos D}{B H_n} \quad (5)$$

$$\frac{\partial N_o}{\partial t} + \frac{\partial N_o}{\partial y}\left(\frac{g \cos D}{\Omega} - \frac{c E_{ox}}{B}\right) = 0 \quad (6)$$

$$\frac{\partial}{\partial y}\left(\Sigma_o \frac{\partial \phi_o}{\partial y}\right) + \frac{2T}{e} \frac{\partial^2 \Sigma_o}{\partial y^2} - \frac{\partial N_o}{\partial y} \frac{g e \cos D}{\Omega} = 0 \quad (7)$$

The equilibrium that we seek exists in the frame drifting with the ions in the y direction, therefore, we transform to a frame drifting with a velocity

$$v_y = \frac{g \cos D}{\Omega} - \frac{c E_{ox}}{B} + \frac{2T}{e} \frac{c \cos D}{B H_n} \quad (8)$$

Equations (5), (6), and (7) become

$$\frac{\partial \Sigma_o}{\partial t} + \frac{\partial \Sigma_o}{\partial y}\left(-\frac{2T}{e} \frac{c \cos D}{B H_n}\right) = \frac{e c g \sin^2 D}{\Omega B H_n} N_o + \Sigma_o \frac{\partial \phi_o}{\partial y} \frac{c \cos D}{B H_n} \quad (9)$$

$$\frac{\partial N_o}{\partial t} + \frac{\partial N_o}{\partial y}\left(-\frac{2T}{e}\frac{c\cos D}{B H_n}\right) = 0 \tag{10}$$

$$\frac{\partial}{\partial y}\left(\Sigma_o \frac{\partial \phi_o}{\partial y}\right) + \frac{2T}{e}\frac{\partial^2 \Sigma_o}{\partial y^2} - \frac{\partial N_o}{\partial y}\frac{g e \cos D}{\Omega} = 0 \tag{11}$$

The first integral of equation (11) yields

$$\frac{\partial \phi_o}{\partial y} = -\frac{2T}{e}\frac{1}{\Sigma_o}\frac{\partial \Sigma_o}{\partial y} + \frac{N_o}{\Sigma_o}\frac{g e \cos D}{\Omega} - \frac{K}{\Sigma_o} \tag{12}$$

which is actually a condition on the east-west component of the current, involving a Pedersen conductivity gradient in the east-west direction.

At this point we assume that the gradient of N is very small. Thus, the gradient of Pedersen conductivity is due largely to a shift in the altitude along a field line of the F region ion density peak as one proceeds in an east-west direction. The integrated Pedersen conductivity increases as the ions on a field line move down the field line to regions where the ion-neutral collision frequency increases because the number of neutrals increase with lower altitude. Using the assumption of small gradients in N and substituting equation (12) into equation (9) yields

$$\frac{\partial \Sigma_o}{\partial t} = \frac{e c g \sin^2 D}{\Omega B H_n} N_o + \frac{c e g \cos^2 D}{\Omega B H_n} N_o - K\frac{c \cos D}{B H_n} \tag{13}$$

$$\frac{\partial N_o}{\partial t} = 0 \tag{14}$$

Setting $\frac{\partial \Sigma_o}{\partial t} = 0$ yields a value for the integration constant K.

$$K = \frac{e g N_o}{\Omega \cos D} \tag{15}$$

Now that it has been shown that an equilibrium exists when there is a gradient of the Pedersen conductivity in the east-west direction, it remains to consider localized perturbations about that equilibrium. These perturbations are of the form $[e^{i(k_x + k_y y - \omega t)}]$, where $k_x, k_y, >> \Sigma_o^{-1} (\partial \Sigma_o / \partial_y)$, and the linearized equations are given as

$$\frac{\partial \Sigma'}{\partial t} + \frac{\partial \Sigma'}{\partial y}\left(-\frac{2T}{e}\frac{c\cos D}{B H_n}\right) + \frac{\partial \Sigma_o}{\partial y}\left(\nabla_x \phi' \frac{c}{B}\right) + \frac{\partial \Sigma'}{\partial x}\left(-\nabla_y \phi_o \frac{c}{B}\right)$$

$$= \Sigma' \frac{\partial \phi_o}{\partial y}\frac{c\cos D}{B H_n} + \Sigma_o \frac{\partial \phi'}{\partial y}\frac{c\cos D}{B H_n} \quad , \tag{16}$$

$$\nabla_\perp \cdot \left(\Sigma_o \nabla_\perp \phi'\right) + \nabla_\perp \cdot \left(\Sigma' \nabla_\perp \phi_o\right) + \frac{\partial \Sigma'}{\partial x}\cos D\left(\frac{2T}{eH_n} + \frac{mg}{e}\right) + \frac{2T}{e}\nabla_\perp^2 \Sigma'$$

$$= 0 \tag{17}$$

where the primes denote perturbed quantities.

Substituting the functional form of the perturbations into equations (16) and (17) yields

$$-i\omega \Sigma' + i k_y \left(-\frac{2T}{e}\frac{\cos D}{B H_n}\right)\Sigma' + i k_x \frac{\partial \Sigma_o}{\partial y}\frac{c}{B}\phi'$$

$$- i k_x \frac{\partial \phi_o}{\partial y}\frac{c}{B}\Sigma' = \Sigma' \frac{\partial \phi_o}{\partial y}\frac{c\cos D}{B H_n} + i k_y \Sigma_o \frac{c\cos D}{B H_n}\phi' \tag{18}$$

and

$$\phi'\left[i k_y \frac{\partial \Sigma_o}{\partial y} - (k_y^2 + k_x^2)\Sigma_o\right] + \Sigma'\left[i k_y \frac{\partial \phi_o}{\partial y} + \frac{\partial^2 \phi_o}{\partial y} + i k_x \frac{\partial \phi_o}{\partial x}\right.$$

$$\left. + i k_x \cos D\left(\frac{2T}{e H_n} + \frac{mg}{e}\right) - \frac{2T}{e}(k_x^2 + k_y^2)\right] = 0 \tag{19}$$

Substituting equation (19) into (18) and assuming $\omega = \omega_r + i\gamma$ yields the expression for the growth rate

$$\gamma = \frac{\partial \phi_o}{\partial y} \frac{c \cos D}{B H_n} + \left[ \frac{k_x}{\Sigma_o} \frac{\partial \Sigma_o}{\partial y} \frac{c}{B} - k_y \frac{c \cos D}{B H_n} \right] \left[ \left( k_x^2 + k_y^2 \right)^2 \right.$$

$$\left. + k_y^2 \left( \frac{1}{\Sigma_o} \frac{\partial \Sigma_o}{\partial y} \right)^2 \right]^{-1} \left\{ (k_x^2 + k_y^2) \left[ k_y \frac{\partial \phi_o}{\partial y} + k_x \frac{\partial \phi_o}{\partial x} \right. \right.$$

$$\left. \left. + k_x \cos D \left( \frac{2T}{e H_n} + \frac{mg}{e} \right) \right] + k_y \frac{1}{\Sigma_o} \frac{\partial \Sigma_o}{\partial y} \left[ \frac{\partial \phi_o}{\partial y} - \frac{2T}{e} (k_x^2 + k_y^2) \right] \right\} \qquad (20)$$

The above expression (20) represents the growth rate for a mode which in general lies at an arbitrary angle to the east west direction. To gain a better physical insight into the phenomena we will restrict our attention to those modes whose wave vectors lie along the x or north-south direction (see Figure 1.b). Thus $k_y = 0$ and

$$\gamma = \frac{c}{B} \left( \frac{B g \cos D}{\Omega c} - E_{ox} \right) \frac{1}{\Sigma_o} \frac{\partial \Sigma_o}{\partial y} - \frac{c}{B H_n} E_{oy} \cos D \frac{\bar{\Sigma}}{\Sigma_o} \qquad (21)$$

where

$$E_{oy} \equiv \frac{e g \sin^2 D}{\Omega \cos D} \frac{N_o}{\bar{\Sigma}} \qquad (22)$$

and it is assumed that the functional form of $\Sigma_o$ is

$$\Sigma_o = \bar{\Sigma} + \Sigma_1(y), \qquad \Sigma_1(y) < \bar{\Sigma}$$

where $\overline{\Sigma}$ is the spatially averaged part of the equilibrium Pedersen conductivity and $\Sigma_1$ contains the east-west spatial variation, the condition that a perturbation grows becomes

$$\frac{c}{B}\left(\frac{g \cos D B}{\Omega c} - E_{ox}\right) \frac{1}{\Sigma_o} \frac{\partial \Sigma_o}{\partial y} \geq \frac{c}{H_n B} \cos D \, E_{oy} \frac{\overline{\Sigma}}{\Sigma_o} \qquad (23)$$

Thus, it has been shown that an equilibrium can exist when an east-west gradient in the Pedersen conductivity is present and that perturbations about that equilibrium with wavevectors in the north-south direction will grow. This equilibrium can be compared with the results of Perkins [1973]. Perkins found that if one chooses an equilibrium of the form

$$\Sigma_o = \text{const}$$

$$N_o = \text{const}$$

$$E_{ox} = \text{const}$$

$$E_{oy} = \frac{e g \sin^2 D}{\Omega \cos D} \frac{N_o}{\Sigma_o}$$

and perturbs about that equilibrium, those modes with wavevectors lying between the zeroth order electric field and the east-west direction would be unstable. The marginally stable mode has a wavevector parallel to the east-west direction.

## III. NUMERICAL SIMULATION RESULTS

The simulations were initialized with perturbations in the north-south direction, as follows:

$$\Sigma(x, y) = \Sigma_o + \Sigma'(x); \tag{24}$$

$$\Sigma_o(y) = \bar{\Sigma}[1 + e^{-2} \sin k_y y],$$

$$k_y \equiv \frac{2\pi}{30 \text{ km}}; \tag{25}$$

$$\Sigma'(x) = \bar{\Sigma} e^{-4} \sin k_x x,$$

$$k_x \equiv \frac{2\pi}{10 \text{ km}}; \tag{26}$$

$$E_{oy} = \frac{eg \sin^2 D}{\Omega \cos D} \frac{N_o}{\bar{\Sigma}}; \tag{27}$$

$$E_{ox} = \tan \theta \, E_{oy}, \tag{28}$$

with $\theta$ given below. The moment equations can be written, after transforming to a frame moving with velocity

$$E_{oy} \frac{c}{B} \hat{e}_x + \left( E_{ox} \frac{c}{B} - \frac{g \cos D}{\Omega} \right) \hat{e}_y \tag{29}$$

and defining

$$\tilde{\Sigma} = \frac{\Sigma(x,y) - \bar{\Sigma}}{\bar{\Sigma}} \equiv \frac{\delta\Sigma}{\bar{\Sigma}} \tag{30}$$

$$\nabla\phi = -\underset{\sim}{E}_o + \nabla\phi' \tag{31}$$

as:

$$\frac{\partial\tilde{\Sigma}}{\partial t} - \nabla\tilde{\Sigma}\cdot(\nabla\phi' \times \hat{z}\frac{c}{B}) = \tilde{\Sigma}(\nabla_y\phi' - E_{oy})\frac{c\cos D}{B H_n} + \nabla_y\phi'\frac{c\cos D}{B H_n} \tag{32}$$

$$\nabla^2\phi' + \frac{\nabla\tilde{\Sigma}}{1+\tilde{\Sigma}}\nabla\phi' + \frac{\frac{\partial\tilde{\Sigma}}{\partial x}}{1+\tilde{\Sigma}}\cos D\left(\frac{2T}{e H_n} + \frac{mg}{e}\right) + \frac{2T}{e}\frac{\nabla\tilde{\Sigma}}{1+\tilde{\Sigma}} - \underset{\sim}{E}_o\cdot\frac{\nabla\tilde{\Sigma}}{1+\tilde{\Sigma}} = 0 \tag{33}$$

The system of equations (32) and (33) for $\tilde{\Sigma}$ and $\phi'$ was solved numerically on an IBM 360/195 computer. The transport equation was solved using a two-dimensional Lax-Wendroff scheme, while the potential was obtained using a modified ADI algorithm. A two-dimensional rectangular 32 x 32 grid with mesh size $\Delta x = \Delta y = 1$ km was chosen. The x and y axes corresponded to the north-south and east-west direction, respectively. The boundary conditions were periodic in both directions. The integrated ion number density was constant throughout

the various simulations (c.f. Perkins, 1973). The parameters chosen for the simulation were: $D = 45^{o}$; $N_o/\Sigma_o = 5 \times 10^{13}/.45 = 1/9 \times 10^{13}$ (mhos - $cm^2)^{-1}$, resulting in $\nu_{in}/\Omega = 2.8 \times 10^{-4}$; $B = 0.5$ gauss; $m = 16\ m_p$ ($m_p$ is the proton mass); $T = 916^{o}K$; $H_n = 55$ km. These parameters were chosen to correspond to an altitude ~350 km (see Johnson, 1961, and Rishbeth and Garriott, 1969).

The results of this investigation are best described within the context of Figures 2 through 5. Figures 2 and 3 show the evolution in time of an F region slab for two cases in which the ratio of north-south to east-west electric field was changed. Figure 2 represents the damped solution f or the case for which

$$H_n \frac{E_{ox}}{E_{oy}} \left| \frac{1}{\Sigma_o} \frac{\partial \Sigma_o}{\partial y} \right|_{max} = \cos D$$

where $E_{oy} = \frac{eg \sin^2 D}{\Omega \cos D} \frac{N_o}{\Sigma}$ and we took $E_{oy} = 4.1$ mV/m and $\theta = 67^{o}$ ($E_{ox} = 1.7$ mV/m). The linear growth rate for this case (where $\frac{1}{\Sigma_o} \frac{\partial \Sigma_o}{\partial y}$ is a maximum) is given as:

$$\gamma = \frac{g \cos D}{\Omega} \frac{1}{\Sigma_o} \frac{\partial \Sigma_o}{\partial y}$$

This situation yields growth only in regions where $\frac{1}{\Sigma_o}\frac{\partial \Sigma_o}{\partial y}$ is positive. This accounts for the slight rippling of the contours seen at the extreme right hand side of the 1450 second plot of Figure 2.

Figure 3 represents a physical situation in which the north-south mode is a growing mode. For this case

$$H_n \quad \frac{E_{ox}}{E_{oy}} \left| \frac{1}{\Sigma_o} \frac{\partial \Sigma_o}{\partial y} \right|_{max} = 9.0$$

Here $E_{oy} = 4.1$ mv/m and $E_{ox} = 21.6$ mV/m ($\theta = 11^o$).

Since $E_{ox} >> g \cos D \, m/e$ the linear growth rate for this case is given approximately as:

$$\gamma = - \frac{c}{B} E_{ox} \frac{1}{\Sigma_o} \frac{\partial \Sigma_o}{\partial y}$$

Therefore, the mode only grows in regions where the gradient in Pedersen conductivity is negative. This is born out in Figure 3.b where growth is exhibited in the central region, i.e., where the initial sinusoidal y variation is favorable.

An important point to note is the development of the smaller scale structures at late times from the initial large scale structures (Figure 3c). This shows that there is a cascading of energy from long wavelength modes to shorter wavelength modes. This cascading of energy and an attendant power law for the power spectrum of the fluctuations is reminiscent of the recent computer simulation results

for type II irregularities in the equatorial E region electrojet given by McDonald et al. [1974]. In both the E region studies and the present F region studies the basic generating mechanism is a form of the $\underline{E} \times \underline{B}$ gradient drift instability (Simon, 1963; 1970; Linson and Workman, 1970). However, in the two cases the dynamical equations governing each region are different. Figure 4 shows the development of $(\delta\Sigma/\bar{\Sigma})_k^2$ for three different modes in the system. The modes labeled 0 and 1 are the east-west and north-south modes, respectively, with which the system was initialized. We note that mode 1 saturates at ~4.8% of the ambient level. The mode labeled 2, however, is the first harmonic of mode 1. Mode 2 is initially lost in the background noise, but eventually appears and grows, indicating that smaller scale structures are developing. Many other shorter wavelength modes develop as the simulation proceeds; however, we chose only to display the first harmonic of mode 1. Figure 5 represents a direction averaged power spectrum for the Pedersen conductivity contours depicted in Figure 3c (t = 669 seconds). A least-squares fit of the numerical simulation results (dots) with a power law curve yielded a $k^{-2}$ spectrum. The falling off of the curve of the short wavelengths is due to the number of grid points used (32x32 km with $\Delta x = \Delta y = 1$ km), i.e., to computer resolution for this particular simulation. This result is in good agreement with the power spectrum obtained by in situ measurements from OGO 6 of ion number density fluctuations made by Dyson et al. [1974]. These authors reported that the square of the amplitude fluctuations obeyed a power law of the form $k^{-n}$ with n close to 2 and an average value of 1.9 for wavelengths between 70m and 7 km.

The power law result from the computer simulation is also in agreement with the power spectrum results deduced by Rufenach [1972] from ionospheric scintillation observations (at Boulder, Colorado)

from the radio source Cygnus A analyzed at 26 MHz. Rufenach showed that the power spectrum for the irregularities in the wavelength regime from 0.6 to 4 km was $\propto k^{-n}$, where n typically varied between 2 and 3. The total $\delta\Sigma/\overline{\Sigma}$ for t = 669 seconds is ~10% which is not at odds with the in situ measurements of Dyson et al. [1974].

A phenomenon associated with spread F is ducting of radio waves along field lines. The presence of localized enhancements and depletions in the background Pedersen conductivity seen in Figure 3 represents a physical situation favorable to ducting of e.m. waves.

## IV. SUMMARY AND DISCUSSION

We have used the nighttime temperate latitude F region equations for field line integrated Pedersen conductivity and potential developed by Perkins [1973] to extend his work to the nonlinear development of a spatially varying ionospheric equilibrium. In particular, we have used a long wavelength variation of Pedersen conductivity in the east-west direction as part of the equilibrium to which we add at $t = 0$ a shorter wavelength north-south perturbation of conductivity. Such a system, under appropriate conditions [see equation (23)], is subject to the usual $\underline{E} \times \underline{B}$ gradient drift instability. The nonlinear evolution of such a system produces a power spectrum for the Pedersen conductivity fluctuations which obeys the relation

$$\left(\frac{\delta\Sigma}{\bar{\Sigma}}\right)^2_k \propto k^{-2} \tag{33}$$

This nonlinear distribution of energy involves a cascade process in which energy is transferred from longer wavelength modes to shorter wavelength modes. This result is in agreement with in situ measurements of F region irregularities Dyson et al. [1974], with observations from scintillation measurements taken at Boulder, Colorado [Rufenach, 1972], and with incoherent scatter measurements from Arecibo [Rino and Livingston, 1974].

The initial orientation of our long wavelength equilibrium and perturbation produces structures, in the nonlinear state, which are sheet-like and more aligned in the east-west direction, i.e., are axially asymmetric in the plane perpendicular to the ambient geomagnetic

field. Such east-west structures have been observed by Singleton [1970] during the winter, at midlatitudes, by using scintillation data from the Explorer 22 beacon experiment. However, at this point the shape of the F region irregularities, determined by scintillation observations, is not entirely clear. A good portion of the time the irregularities appear to be axially symmetric (Singleton, 1970; Moorcroft and Arima, 1972). Moorcroft and Arima [1972] also give evidence for elongation more in the north-south direction as does Singleton [1970] for seasons other than winter (it should be pointed out that Moorcroft and Arima's data was not taken in winter and so is not inconsistent with Singleton's findings). Our computer simulation results, Figure 3, would depict an average $\underline{k}$ for the final state more in the north-south direction. Phase space plots in k space support this idea, i.e., that the final power spectrum has a preferential direction (north-south). This is unlike the numerical simulation results of the type II equatorial E region irregularities which show that the $\underline{k}$ vectors are isotropized in the final state (see McDonald et al. 1974b). This is probably due to Hall current effects which operate effectively in the E region but not in the F region. For the initial conditions chosen for our simulation, this implies more of a one-dimensional steepening process rather than a true two-dimensional turbulence process (as is the case of type II equatorial E region irregularities; see McDonald et al. 1974a) for the resulting nonlinear quasi-final state. We believe that if we choose a long wavelength north-south equilibrium and a perturbation in the east-west direction, the resulting nonlinear development of the $\underline{E} \times \underline{B}$ instability would show a north-south preference. We are continuing further studies along these lines. Moorcroft and Arima [1972] have pointed out, in a qualitative fashion, that the $\underline{E} \times \underline{B}$ gradient drift instability is a good candidate for the axial asymmetry.

We do not wish to imply that our results can explain all spread F observations. Rather, we have shown how the $\underline{E} \times \underline{B}$ instability, using Perkins'[1973] F region equations, can produce F region irregularities which are in agreement with certain aspects of the observations of these irregularities. Perkins' instability mechanism had a growth rate proportional to $\nu_{in}^{-1}$ (not an $\underline{E} \times \underline{B}$ instability, since his initial equilibrium had a constant value for the F region Pedersen conductivity). He compared his results with experimental observations of spread F (see Herman, 1966 for a comprehensive review of spread F). He concluded, based on linear theory, that the mechanism was in agreement with spread F observations. Perkins' instability mechanism required a north-south electric field, as does our mechanism. His instability, being inversely proportional to the F region ion-neutral collision frequency, favored instability when the F layer was high. Our instability criterion, equation (23), while involving the north-south and the east-west electric field, also involves the neutral scale height, $H_n$ (this comes from Perkins' model equations where the ion-neutral collision frequency is taken as having exponential dependence with this scale height). The condition shows that for a fixed ratio of electric fields the instability is stronger for larger values of $H_n$, i.e., increasing F region altitudes. Also of interest is the fact that neither instability mechanism makes use of a vertical gradient in ion density.

In concluding, we have shown by a numerical simulation following Perkins' [1973] nighttime F region equations in time into the nonlinear regime, that F region irregularities can be produced via the usual $\underline{E} \times \underline{B}$ instability. However, we believe that further work on the generation and nonlinear development of F region irregularities is warranted in order to gain an improved understanding of the relationship between these irregularities, spread F and scintillation phenomena.

## ACKNOWLEDGMENTS

This work was supported by NAVAIR. The authors are grateful to Dr. J. A. Fedder for many valuable discussions.

## REFERENCES


Dyson, P. L., J. P. McClure, and W. B. Hanson, "In Situ Measurements of the Spectral Characteristics of F Region Ionospheric Irregularities," J. Geophys. Res., 79, 1497, 1974.

Herman, J. R., "Spread F and Ionospheric F Region Irregularities," Rev. Geophys. Space Phys., 4, 255, 1966.

Johnson, F. S., Satellite Environment Handbook, Stanford University Press, 1961, pgs. 19-21.

Linson, L. M. and J. B. Workman, "Formation of Striations in Ionospheric Plasma Clouds," J. Geophys. Res., 75, 3211, 1970.

McDonald, B. E., T. P. Coffey, S. Ossakow and R. N. Sudan, "Preliminary Report of Numerical Simulation of Type II Irregularities in the Equatorial Electrojet," J. Geophys. Res., 79, 2551, 1974a.

McDonald, B. E., T. P. Coffey, S. L. Ossakow, and R. N. Sudan, "Numerical Studies of Type II Equatorial Electrojet Irregularity Development," Radio Sci. (in press), 1974b.

Moorcroft, D. R. and K. S. Arima, "The Shape of the F-Region Irregularities which Produce Satellite Scintillations - Evidence for Axial Asymmetry," J. Atmos. Terr. Phys., 34, 437, 1972.

Perkins, F. W., "Spread F and Ionospheric Currents," J. Geophys. Res., 78, 218, 1973.

Rino, C. L., and R. C. Livingston, "Incoherent Scatter Measurements of Ionospheric Irregularity Spectra," Trans. Am. Geophys. Un., 56, 1155, 1974.

Rishbeth, H. and O. K. Garriott, Introduction to Ionospheric Physics, Academic, New York, 1969, pgs. 118-119, 131, and 171.

Rufenach, C. L., "Power-Law Wavenumber Spectrum Deduced from Ionospheric Scintillation Observations," J. Geophys. Res., 77, 4761, 1972.

Simon, A., "Instability of a Partially Ionized Plasma in Crossed Electric and Magnetic Fields," Phys. Fluids, 6, 382, 1963.

Simon, A., "Growth and Instability of Artificial Ion Clouds in the Ionosphere," J. Geophys. Res., 75, 6287, 1970.

Singleton, D. G., "Dependence of Satellite Scintillations on Zenith Angle and Azimuth," J. Atmos. Terr. Phys., 32, 789, 1970.

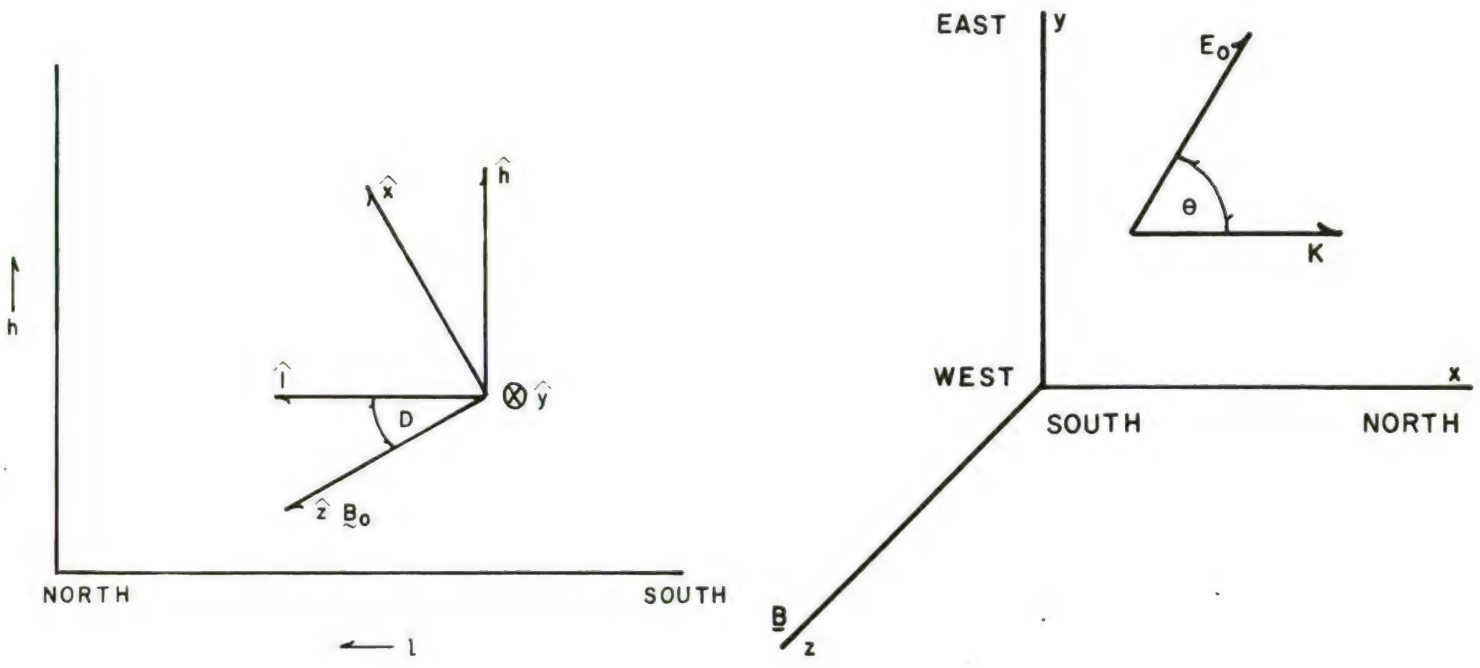


Fig. 1 — Geometry for F region studies, (a) this is an eastward view in a northern hemisphere magnetic meridian plane. The unit vectors $\hat{\ell}$ and $\hat{h}$ are in the horizontal and vertical directions, respectively; whereas, the unit vectors $\hat{z}$ and $\hat{x}$ are parallel and perpendicular to the geomagnetic field $\underline{B}_o$. The relations between the quantities are $h = x \cos D - z \sin D$, $\ell = x \sin D + z \cos D$, where D is the dip angle which the magnetic field makes with the horizontal, $\hat{\ell}$, and (b) orientation of ambient electric field, $\underline{E}_o$ and wave vector, $\underline{k}$, for initial perturbation considered in this paper.

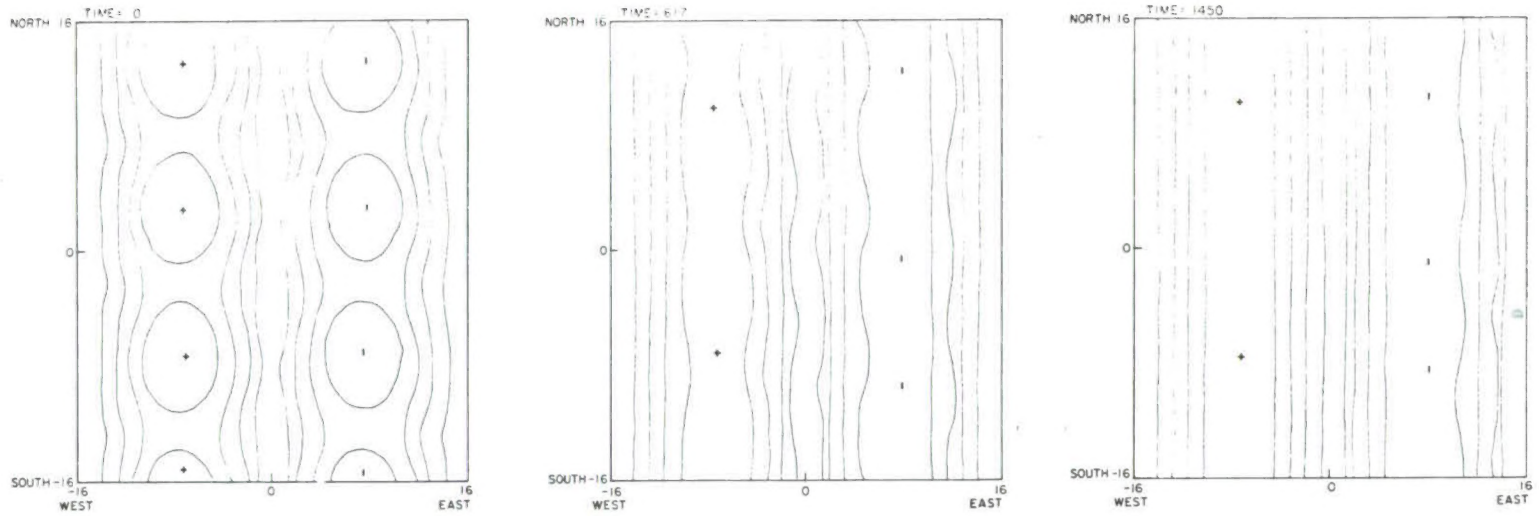


(a) (b) (c)

Fig. 2 — Iso-Pedersen conductivity contours at time (a) 0, (b) 617 seconds, and (c) 1450 seconds. This case is for $E_{ox}$ = 1.7 mV/m and $E_{oy}$ = 4.1 mV/m and shows essentially no growth. The contour spacing is 3, 6, 9, and 12% above the spatially averaged constant background, and the plus and minus represent extrema above and below this background. The individual frames are slices of the F region ionosphere which in this case is 32 × 32 km.

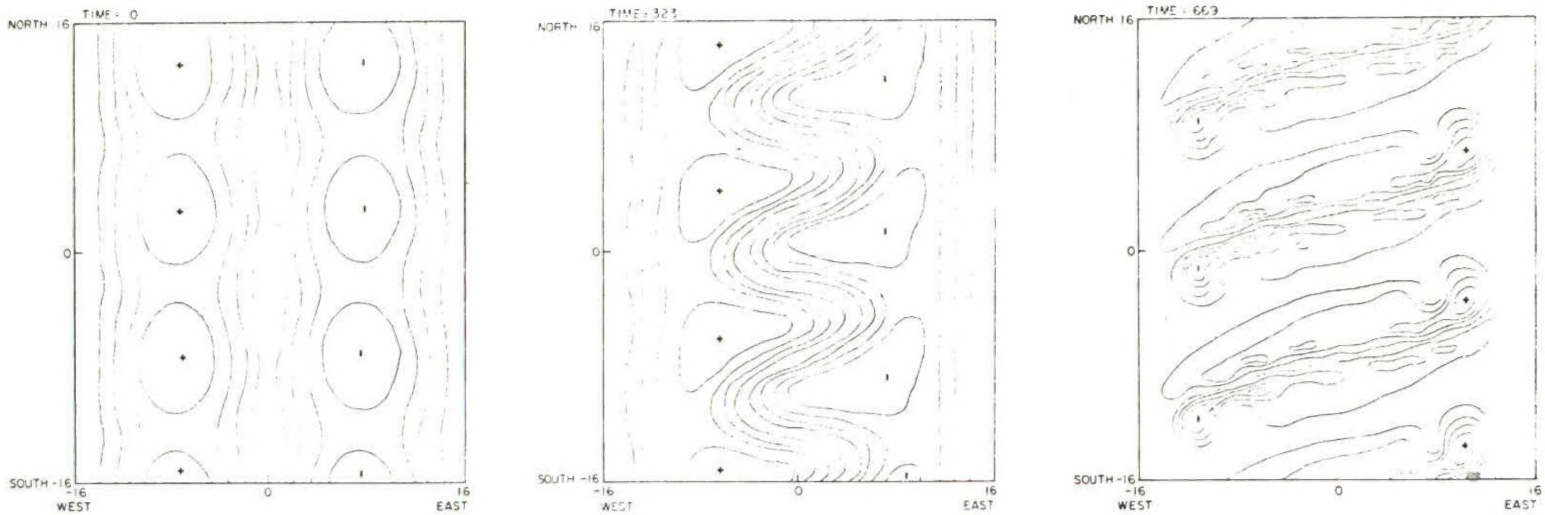


(a) (b) (c)

Fig. 3 — Pedersen conductivity level contours at times (a) 0, (b) 323 seconds, and (c) 669 seconds for $E_{ox}$ = 21.6 mV/m and $E_{oy}$ = 4.1 mV/m. This shows strong instability in the central region. The contour spacing at t = 0 is the same as in Fig. 2, but then the contours become larger in value as time progresses.

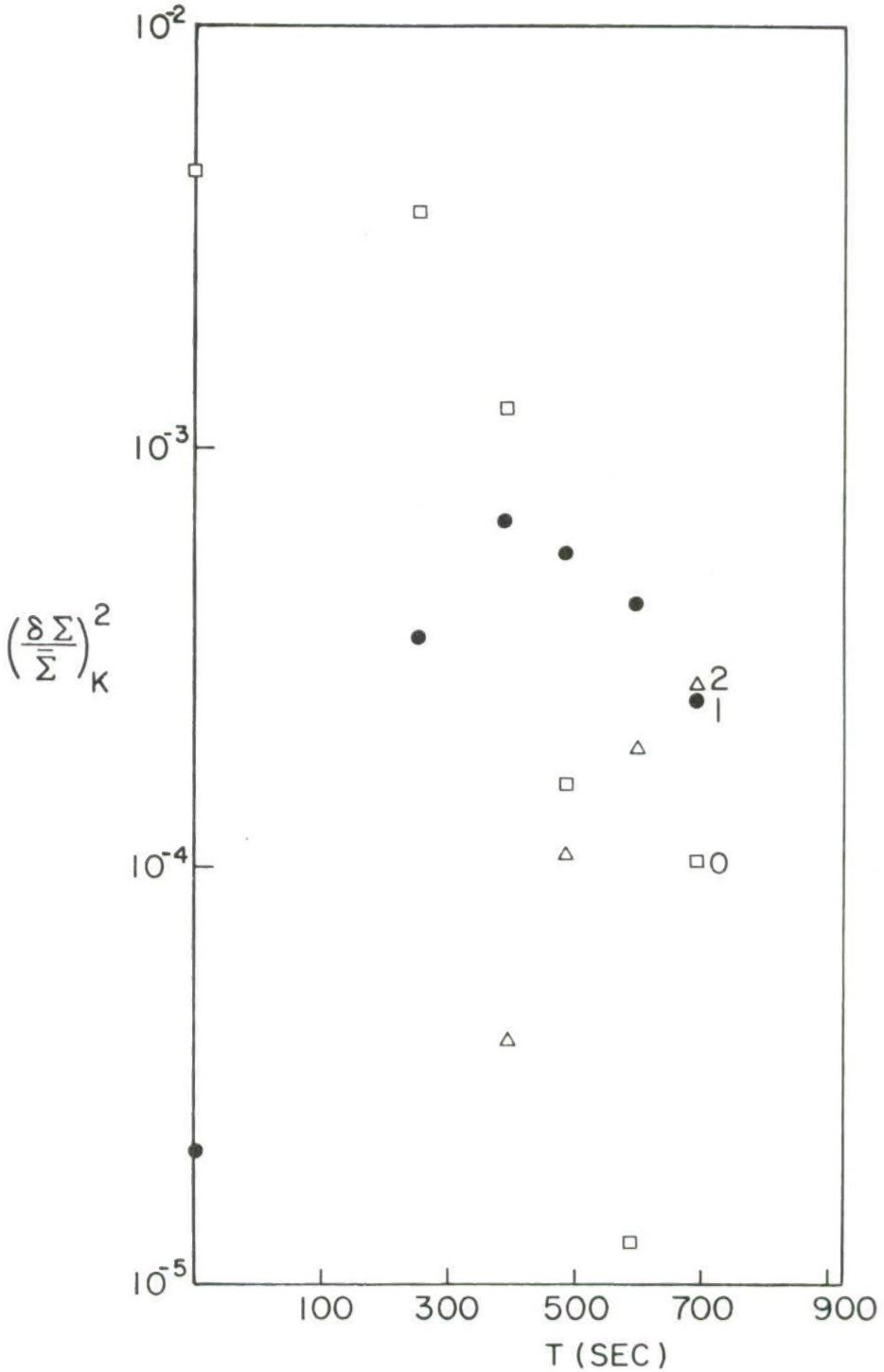


Fig. 4 — Pedersen conductivity fluctuation amplitude squared for several modes as a function of time for the case depicted in Fig. 3. The main initial east-west long wavelength spatial variation is labeled 0 (squares) and the initial shorter wavelength north-south perturbation is labeled 1 (dots). The label 2 (triangles) is the second harmonic of 1.

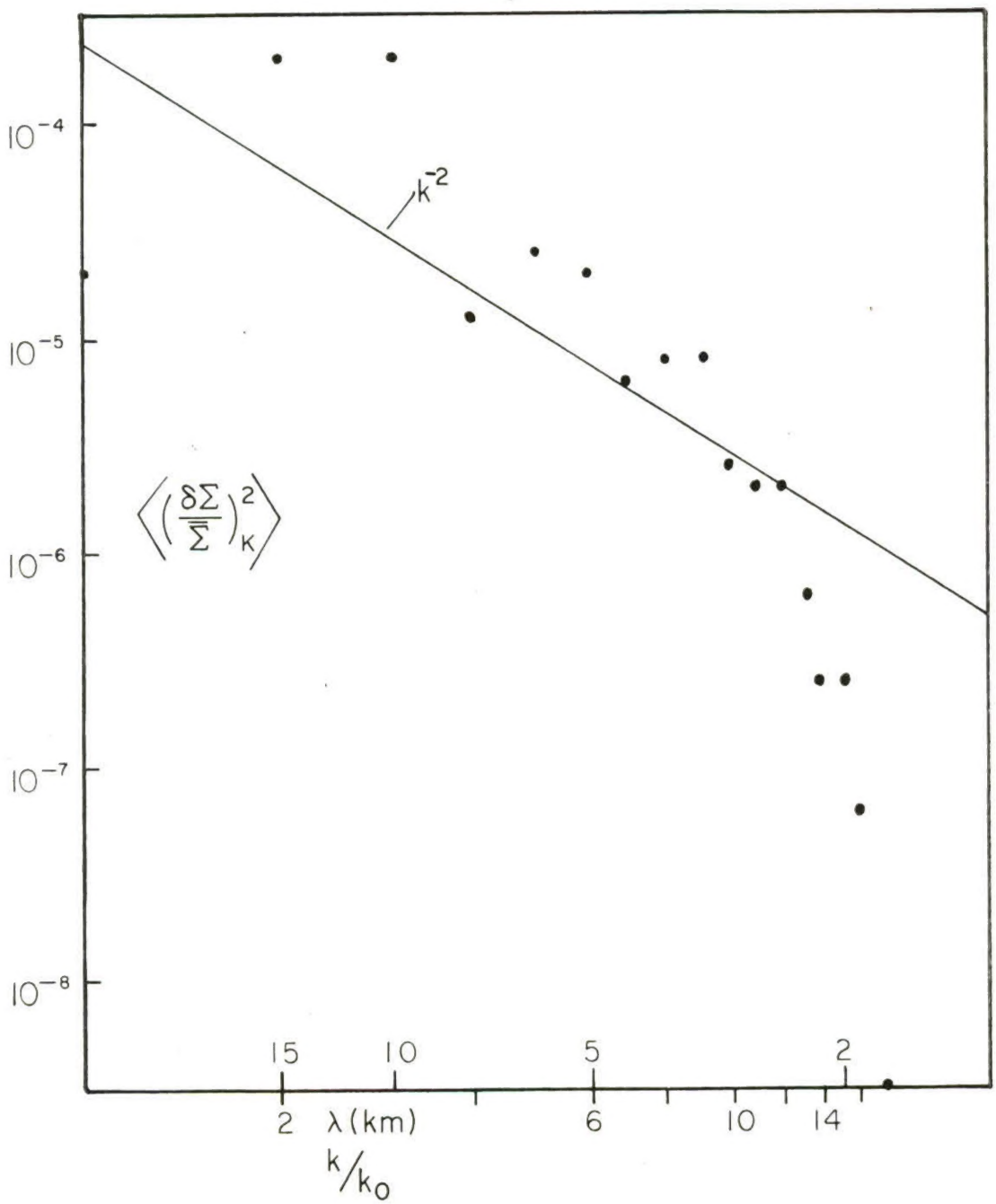


Fig. 5 — Direction-averaged power spectrum of the Pedersen conductivity fluctuations at 669 seconds depicted in Fig. 3, plotted on a log-log scale. On the wavenumber scale, $k_0$ is the initial long wavelength east-west variation. The power law $k^{-2}$ was obtained by a weighted least squares fit to the simulation results (dots).